Journal of Power Sources 268 (2014) 279–286

Contents lists available at ScienceDirect

Journal of Power Sources

journal homepage: www.elsevier.com/locate/jpowsour

Ab initio characterization of layered MoS_2 as anode for sodium-ion batteries

Majid Mortazavi [a], Chao Wang [a], Junkai Deng [a, b], Vivek B. Shenoy [c], Nikhil V. Medhekar [a, *]

[a] Department of Materials Engineering, Monash University, Clayton, Victoria 3800, Australia
[b] State Key Laboratory for Mechanical Behavior of Materials, Xi'an Jiaotong University, Xi'an, China
[c] Department of Materials Science and Engineering, University of Pennsylvania, Philadelphia, PA 19104, USA

HIGHLIGHTS

- We characterize layered MoS_2 as an anode for sodium-ion batteries.
- The strong binding of Na with MoS_2 is favorable against Na cluster formation.
- Sodiation induces a phase transformation from hexagonal to tetragonal phase.
- We found the maximum capacity of 146 mAh g^{-1} and average electrode potential of 0.75–1.25 V for Na intercalation in MoS_2.
- The result on Na diffusion barrier in MoS_2 suggests a moderately fast mobility.

GRAPHICAL ABSTRACT

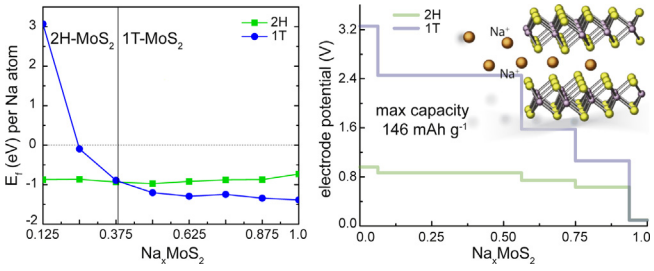

ARTICLE INFO

Article history:
Received 25 March 2014
Received in revised form
8 June 2014
Accepted 9 June 2014
Available online 18 June 2014

Keywords:
Sodium-ion batteries
Anodes
Transition metal dichalcogenides
Molybdenum disulphide
Density functional theory

ABSTRACT

Identifying suitable layered materials as electrodes with desirable electrochemical properties remains a key challenge for rechargeable Na-ion batteries (NIBs). Using first principles methods, here we examine the efficacy of layered molybdenum disulphide (MoS_2) as a host electrode material for NIBs. We identify various low energy Na adsorption sites and evaluate the stability of the hexagonal and tetragonal polytypes of MoS_2 upon Na intercalation. Our results illustrate a moderately strong binding between Na and MoS_2 that is thermodynamically favorable against the cluster formation and phase separation of Na. We find that while Na intercalation in MoS_2 results in a phase transformation from the hexagonal phase to the tetragonal phase, it gives rise to a maximum theoretical capacity of 146 mAh g^{-1} and a low average electrode potential in the range of 0.75–1.25 V. Our calculations of Na diffusion kinetics indicates a moderately fast mobility of Na in the van der Waals interlayer spaces of MoS_2. These results highlight the promise of MoS_2 as an appealing negative electrode (anode) for rechargeable NIBs.

1. Introduction

Rechargeable Na-ion batteries (NIBs) are rapidly emerging as a plausible alternative to Li-ion batteries (LIBs), particularly for stationary grid-based energy storage [1–3]. This growing interest in NIBs can be attributed not only to the abundance of Na and the associated cost advantages, but also to its low electronegativity

* Corresponding author. Tel.: +61 3 9905 1421; fax: +61 3 9905 4940.
E-mail address: nikhil.medhekar@monash.edu (N.V. Medhekar).

http://dx.doi.org/10.1016/j.jpowsour.2014.06.049
0378-7753/

which is next only to Li among alkali metals. An increasing number of experimental and theoretical studies have investigated a wide range of Na-ion battery chemistries in pursuit of desirable electrochemical capacities, an appropriate voltage range and a long cycle life [1,2]. A significant part of this effort is focused on identifying suitable van der Waals-bonded layered materials that can act as negative electrodes (anodes) of NIBs [2]. In contrast to the potential materials such as Sn and Pb which offer large capacities but poor mechanical stability [4], layered materials can intrinsically accommodate guest ions within the van der Waals spacing with a minimum structural distortion and allow for their fast transport during charging and discharging cycles. In state of the art LIBs, graphitic carbon is the most commonly used layered material for anodes [2]. Li forms an intercalation compound LiC_6 with graphite at full charge with a maximum capacity in excess of 340 mAh g^{-1} [5]. However, due to the larger size of Na ion (1.02 Å vs. 0.76 Å for Li), Na intercalation in graphite is highly inefficient—Na can only form an eighth-stage intercalation compound NaC_{64} with graphite with a very poor capacity [6].

Among the non-carbon layered materials that are being explored as effective electrode materials for NIBs, titanates and titanium phosphates have demonstrated a maximum capacity in the range of 100–140 mAh g^{-1} [2,3]. However, a large class of layered materials, namely, transition metal dichalcogenides remains relatively unexplored as a potentially useful alternative to graphite for anodes of NIBs. These materials (with chemical formula MX_2, where M is a group IV, V or VI transition metal such as Mo, W and Ti, and X is a chalcogen such as S, Se and Te) are of interest for a broad range of applications in hydrogen storage, catalysis, and more recently, in optoelectronic devices [7,8]. Similar to graphite, the atomic structure of this family of materials is characterized with a strong in-plane and a weak out-of-plane bonding [9,10]. Moreover, transition metal dichalcogenides have a larger interlayer spacing than graphite, and offer a wide range of electron affinity for the intercalation of a guest electronegative ion [11].

While this ability to readily intercalate guest ions has been greatly exploited for exfoliating these layered structures into individual layers [12], attempts to employ transition metal dichalcogenides as active electrode materials for rechargeable batteries have been few, and so far, largely limited to LIBs [13–15]. Recently, Park et al. demonstrated electrochemical insertion of Na in layered molybdenum disulphide (MoS_2) with a steady state capacity of 85 mAh g^{-1} after 100 charge–discharge cycles [16]. Similarly, studies have also reported a specific capacity in the range of 50–140 mAh g^{-1} for Nb [17], W [18], and Ti [19] disulphides. While these initial studies report moderate capacities of transition metal dichalcogenides for Na, very recent experiments have shown that they can be further enhanced to 250–350 mAh g^{-1} by using composites. For instance, the work of David et al. [20] and Bang et al. [21] demonstrated that when a composite of MoS_2 with graphene oxide is employed as an active anode, the maximum capacity of 230 and 360 mAh g^{-1}, respectively, could be achieved. These experiments point to the feasibility of layered transition metal dichalcogenides as high capacity anode materials for NIBs, however, an atomic level understanding of Na intercalation processes in these materials is not yet available. The knowledge of structural stability of Na-intercalated transition metal dichalcogenides, their electronic properties and electrochemical characteristics over a wide compositional range is essential in determining their viability as electrode materials for NIBs.

In this work, we systematically investigate Na intercalation in layered MoS_2 as a representative example of layered transition metal dichalcogenide anode for NIBs. We consider all possible structural polytypes that have been typically reported for crystalline MoS_2. In its natural state, MoS_2 is generally found in its most stable form with a hexagonal 2H crystal structure [11], while a high energy tetragonal 1T polytype can also be stabilized via liquid-state exfoliation [22]. Moreover, several experimental and theoretical studies have pointed out a coexistence of 2H crystal symmetry with a closely related rhombohedral 3R symmetry [23,24], while a few studies have also investigated a hypothetical tetragonal 2T structure [25]. Using first principles density functional theory calculations, here we analyze the structural stability, electronic structure, and intercalation voltages for Na intercalation compounds with 2H, 3R, as well as 1T and 2T polytypes of MoS_2. We find that Na intercalation in MoS_2 leads to a structural phase transformation from the hexagonal to the tetragonal polytype, and further, all intercalated compounds remain largely metallic irrespective of the structural polytype. We obtain crucial electrochemical properties such as average operating voltage, theoretical capacity and Na diffusion barriers, and evaluate the feasibility of layered MoS_2 as an effective anode material for NIBs.

2. Methodology

Schematic representations of the crystal structures for the 2H, 3R, 1T and 2T MoS_2 polytypes considered in our study are shown in Fig. 1. Both 2H and 3R polytypes are characterized by a trigonal prismatic D_{3h} coordination, while 1T and 2T polytypes have an octahedral O_h coordination [11]. MoS_2 layers in 2H, 3R, 1T and 2T polytypes are arranged in antiparallel *AB*, parallel *ABC*, parallel *AA*, and antiparallel *AA′* stacking sequence, respectively. For all these crystal symmetries, we performed first principles total energy calculations within the framework of spin-polarized density functional theory (DFT) using Vienna Ab initio Simulation Package (VASP) [26]. We used the generalized gradient approximation of the Perdew–Burke–Ernzerhof form to describe electron exchange and correlation [27], while the core and valence electronic interactions were modeled using projector augmented wave potentials [28]. The electrons in $2p^6 3s^1$, $4p^6 5s^1 4d^5$, $2s^2 3p^4$ states were treated as valence electrons for Na, Mo and S, respectively. Since the standard generalized gradient approximation underestimates interlayer van der Waals interactions, we employed Grimme's energy correction method to correctly account for these dispersion interactions [29]. A 17 × 17 × 11 *k*-point mesh per MoS_2 unit for sampling the Brillouin zones was used to ensure the variation in total energy is less than 1 meV/atom. In each case, we used a plane wave kinetic energy cut off of 500 eV. The optimized structures were obtained by allowing both the cell vectors as well as ionic positions to fully relax until the Hellmann-Feynman forces were less than 0.01 eV $Å^{-1}$.

Our calculated optimized lattice parameters for all MoS_2 polytypes are tabulated in Table S1, SD. The obtained lattice parameters for all polytypes are in good agreement with experimental and theoretical values reported earlier [11,25,30]. Consistent with experimental observations, we found that 2H is energetically the most favorable polytype of MoS_2 (see Table S1 in SD) [24]. Finally, we also computed total density of states for all polytypes of MoS_2 and found that 2H and 3R polytypes are semiconductors with 0.9 eV and 0.92 eV band gap, respectively, while 1T and 2T polytypes are metallic (Fig. S1 in SD). These observations are also consistent with earlier reports investigating the electronic structure of transition metal dichalcogenides [31,32]. To obtain optimized geometries and energies of Na intercalation compounds with MoS_2, Na atoms were first inserted in the interlayer spacings to form the compound Na_xMoS_2, and the composite Na-intercalated structure was reoptimized. The binding energy for Na in layered MoS_2 was then calculated using the expression $E_b(x) = E(Na_xMoS_2) - E(MoS_2) - x\,E(Na)$, where $E(Na_xMoS_2)$ is the total energy of the Na_xMoS_2 compound, $E(MoS_2)$ is the total energy

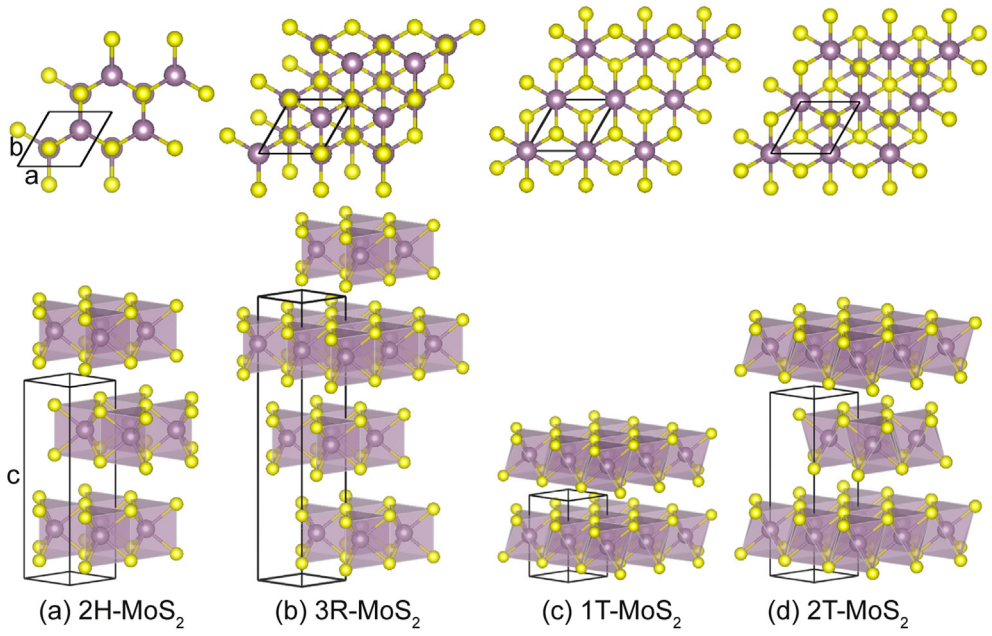

Fig. 1. Structural polytypes of layered MoS_2: (a) 2H, (b) 3R, (c) 1T and (d) 2T. *a*, *b* and *c* denote the lattice constants of the hexagonal unit cell. Yellow and purple spheres represent S and Mo atoms, respectively. (For interpretation of the references to color in this figure legend, the reader is referred to the web version of this article.)

of the same MoS_2 polytype and E(Na) is the energy of Na atom in its gaseous state. According to this definition, a negative binding energy indicates an exothermic chemical interaction between Na and MoS_2.

3. Results and discussion

3.1. Na adsorption sites and energetics of intercalation in MoS_2

To systematically study Na intercalation in layered MoS_2, we first examined low energy adsorption or binding sites for an isolated Na atom in the interlayer van der Waals spacing. We identified two distinct Na binding sites irrespective of the MoS_2 polytype, namely, (a) an octahedral site, where Na is bonded to six nearest sulfur atoms, (b) a tetrahedral site, where adsorbed Na is bonded to four nearest sulfur atoms. These binding sites are schematically illustrated in Fig. 2. We find that among these sites, the adsorption of an isolated Na is more favorable in octahedral site—Na binding energy at the octahedral site is generally lower by 80–300 meV than at the tetrahedral site.

Next we investigated the concentration dependence of Na intercalation in all four polytypes of MoS_2 using a fully periodic supercell consisting of at least two MoS_2 layers, each containing four MoS_2 units. Using such a large supercell allows us to consider Na_xMoS_2 compounds with eight distinct chemical compositions (x = 0.125, 0.25, 0.375, 0.5, 0.625, 0.75, 0.875 and 1). Since Na ordering can be different for different Na concentrations, we considered all possible configurations for every composition considered. In all configurations, Na atoms were initially distributed in either octahedral or tetrahedral sites as far away from each other as possible in order to minimize their self-interaction. For each configuration, the structure was then fully optimized. The Na ordering that gives the lowest binding energy for each concentration, the ground state, was chosen for further electrochemical analysis. Our calculations show that both geometrical characteristics and the energetics of Na-intercalated 3R and 2T MoS_2 are almost identical to the geometry and the energetics of 2H and 1T polytype, respectively. This observation suggests that the weak dispersion interactions that distinguish 2H and 3R polytypes, as well as 1T and 2T polytypes, are negligible compared to the strong chemical interactions between Na and MoS_2. Therefore, here we present the results for Na intercalation in 2H- and 1T-MoS_2 as representative MoS_2 polytypes, while key the results for 3R and 2T MoS_2 polytypes are summarized in the SD.

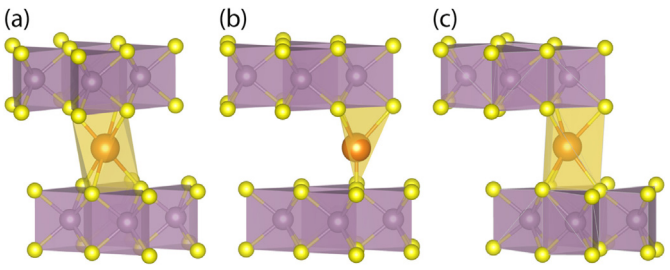

Fig. 2. Schematic illustration of three distinct binding sites for Na in the interlayer spacing of MoS_2: (a) octahedral, (b) tetrahedral, and (c) distorted-octahedral. Orange spheres represent Na atoms. (For interpretation of the references to color in this figure legend, the reader is referred to the web version of this article.)

Fig. 3 shows Na binding energy across the entire composition range for various stable binding configurations within 2H- and 1T-MoS_2. It also presents a convex hull for the binding energies (black lines), representing lowest energy binding sites in both 2H and 1T polytypes. Interestingly, in addition to the octahedral and tetrahedral binding sites, we also identified a distinct distorted-octahedral Na binding site in several configurations. The distorted-octahedral binding site is structurally close to the octahedral site but with a Na–S polyhedron that is distorted from its original octahedral shape due to a relative sliding of S atomic plane (see Fig. 2c). It is evident that Na binding energies for all configurations in 2H- and 1T-MoS_2 polytypes are negative, indicating an energetically favorable chemical interaction between Na and layered MoS_2. At low ($x \leq 0.25$) and full ($x = 1$) Na concentrations in 2H-Na_xMoS_2, octahedral sites provide lowest energy configurations, while

tetrahedral sites correspond to the metastable configurations. In contrast, for intermediate concentrations in 2H-MoS_2, distorted-octahedral sites provide the energetically most favorable Na binding configurations. On the other hand for nearly all Na concentrations in 1T-MoS_2, distorted-octahedral sites are found to be energetically most favorable. Fig. 3 in SD shows the lowest energy configurations of both 2H- and 1T-Na_xMoS_2, while their optimized lattice parameters are summarized in Table 1.

While Na binding energies in 2H- and 1T-MoS_2 are negative for all concentrations as shown in Fig. 3, it is clear that Na binds more strongly to 1T-MoS_2 than to 2H-MoS_2—Na binding energies in 1T-MoS_2 are generally lower by 1.1–1.9 eV than the binding energies in 2H-MoS_2. The stronger Na binding with the 1T polytype can be explained by the crystal field theory that describes a symmetry-induced splitting of Mo-4*d* orbitals in various MoS_2 polytypes [33,34]. In 2H-MoS_2, since the lowest energy Mo – $4d_z^2$ orbital of the D_{3h}-MoS_6 unit is fully occupied, an electron from donor Na can only be accommodated in the higher energy $4d_{xy}$ and $4d_{x^2-y^2}$ orbitals. In contrast, the lowest energy degenerate $4d_{xy}$, $4d_{yz}$ and $4d_{xz}$ orbitals in 1T-MoS_2 are partially occupied and can readily accommodate the electron from Na, leading to a large negative binding energy. Nevertheless, it should be emphasized that Na binding energies for all concentrations in both 2H and 1T-MoS_2 polytypes are much lower than the cohesive energy of Na (−1.11 eV per atom). This observation suggests a strong driving force for the adsorption of Na within the interlayer spaces of MoS_2 and against the formation of Na clusters which can be detrimental to the performance of electrochemical cells. Our obtained Na binding energies therefore point to a thermodynamic suitability of layered MoS_2 as an electrode material for NIBs.

3.2. Lattice deformation upon Na intercalation

It has been established that repetitive structural changes associated with ion intercalation and deintercalation can lead to capacity fade and a loss of electrochemical performance of the electrodes [35]. To investigate the influence Na intercalation on the stability of the crystalline structure of layered MoS_2, we have analyzed the variation of lattice parameters with Na concentration as shown in Fig. 4. We find that for both hexagonal and tetragonal polytypes, the lattice parameter *a* increases only marginally in the range of 6.4–6.8 Å over the entire concentration range. In contrast, the effect of Na intercalation on the lattice parameter *c* is more significant. As Na enters the van der Waals interlayer spaces, *c* rapidly rises during the second ($x = 0.125$) and the first ($x = 0.25$) stage of Na intercalation, and fluctuates in a narrow range upon further increasing Na concentration. These small fluctuations are associated with both interlayer and intralayer the Na–Na interactions. As a consequence of interlayer expansion, Na intercalation leads to a volume expansion of 27% at full concentration. It should be noted that while this magnitude of volume expansion is apparently large, Na intercalation in MoS_2 in the concentration range $0 < x < 1$ is mainly contributed by the expansion of interlayer van der Waals space, and not due to any bond breaking in the host material. This behavior is in contrast with intercalation in the bulk high capacity materials for rechargeable batteries (such as silicon and tin), where the intercalation of the guest ion induces bond breaking and a subsequent capacity loss in the host material [36–39].

Table 1
Optimized lattice parameters (*a*, *b*, *c*, *α*, *β*, *γ*), minimum in-plane Na–Na distance (d_{Na-Na}), formation energy (E_f) and net charge on Na (*q*) for Na-intercalated MoS_2.

x	*a*,*b* (Å)	*c* (Å)	*α* (°)	*β* (°)	*γ* (°)	d_{Na-Na} (Å)	E_f (eV)	*q* (ē)
2H-Na_xMoS_2								
0.000	6.39	12.40	90	90	60	–	–	–
0.125	6.42	13.58	90	90	60	6.42	−0.11	0.86
0.250	6.44	14.87	90	90	60	6.44	−0.21	0.85
0.375	6.43	15.27	78	77	60	5.46	−0.33	0.84
0.500	6.44	14.84	90	90	60	3.19	−0.47	0.85
0.625	6.51	15.10	90	102	60	3.25	−0.56	0.83
0.750	6.54	14.68	90	90	60	3.20	−0.66	0.83
0.875	6.60	14.98	102	89	60	3.21	−0.72	0.82
1.000	6.58	14.87	90	90	60	3.29	−0.73	0.78
1T-Na_xMoS_2								
0.000	6.46	12.06	90	90	60	–	–	–
0.125	6.52	13.56	90	90	60	6.52	0.38	0.87
0.250	6.57	14.35	90	96	60	6.50	0.01	0.87
0.375	6.58	14.10	88	91	60	3.18	−0.26	0.86
0.500	6.60	14.26	89	95	60	3.23	−0.53	0.85
0.625	6.67	14.28	88	88	59	3.31	−0.73	0.84
0.750	6.74	14.49	76	76	60	2.99	−0.92	0.84
0.875	6.77	14.06	89	89	59	3.21	−1.17	0.83
1.000	6.82	14.33	103	89	60	3.37	−0.83	0.82

3.3. Phase transformation in layered MoS_2 upon Na intercalation

Next we evaluate the relative stability of various MoS_2 polytypes upon Na intercalation. It is well known that among all MoS_2 polytypes, 2H-MoS_2 is the most stable form of MoS_2. We therefore define the formation energy for all Na_xMoS_2 intercalation compounds with respect to 2H-MoS_2 and Na body centered cubic crystal as the reference states, as $E_f(x) = E(Na_xMoS_2) - E(2H - MoS_2) - xE(Na^{bcc})$, where $E(Na_xMoS_2)$ is the energy of Na_xMoS_2 compound per MoS_2

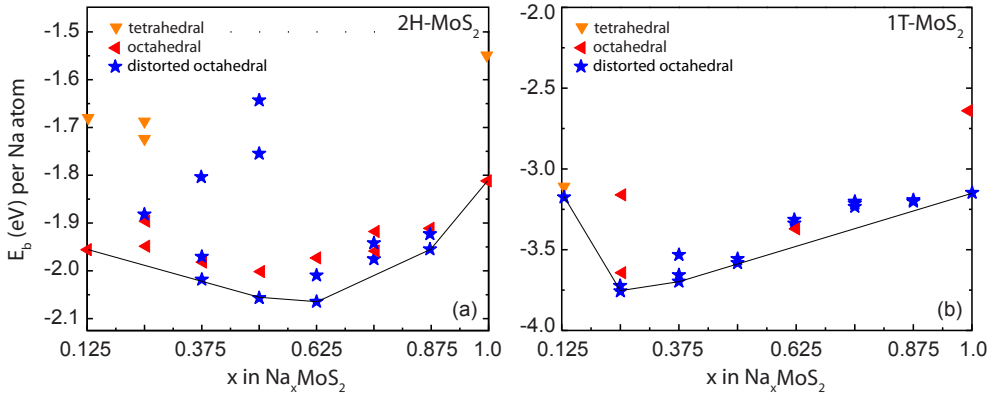

Fig. 3. The convex hull of Na binding energies for (a) 2H- and (b) 1T-Na_xMoS_2. Distinct binding energies for the same chemical composition of Na_xMoS_2 indicate metastable Na binding configurations.

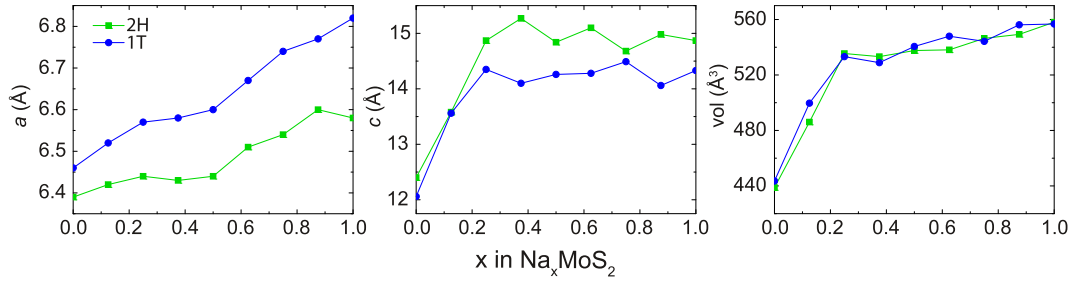

Fig. 4. Variation of the lattice parameters and the cell volume with Na concentration for 2H- and 1T-Na_xMoS_2 intercalation compounds.

formula unit, $E(2H-MoS_2)$ is the energy of 2H-MoS_2 per MoS_2 formula unit, and $E(Na^{bcc})$ is the energy per atom of Na in the body centered cubic crystal. A negative value of the formation energy indicates a thermodynamic stability of the intercalation compound against the separation into most stable forms of both MoS_2 and Na. The calculated values of the formation energy for the lowest energy configurations for 2H-Na_xMoS_2 and 1T-Na_xMoS_2 are presented in Table 1, while Fig. 5 shows the variation of the formation energy per Na as a function of the concentration x. It can be seen that 2H-MoS_2 is stable upon Na intercalation over the entire concentration range, while 1T polytype is stable only beyond concentration $x > 0.25$. More interestingly, for Na concentrations larger than $x = 0.39$, the formation energy of 1T-Na_xMoS_2 is lower than that of 2H-Na_xMoS_2, indicating a phase transformation from 2H to 1T polytype at $x = 0.39$. This phase transformation is qualitatively similar to the observations reported in earlier studies on the intercalation-induced phase transformation in transition metal dichalcogenide nanotubes and multilayers [33,34,40]. These studies showed that the phase transformation can be attributed to a modification of Mo-d orbitals that stabilizes octahedral Mo coordination of the 1T phase at large concentrations of the intercalating electron donors. Recent real-time high resolution microscopy experiments have revealed the mechanism that such phase transformations, which involves gliding of the S atomic plane in two stages, namely, nucleation of 1T phase and growth of 1T phase via migration of two different domain boundaries [41,42].

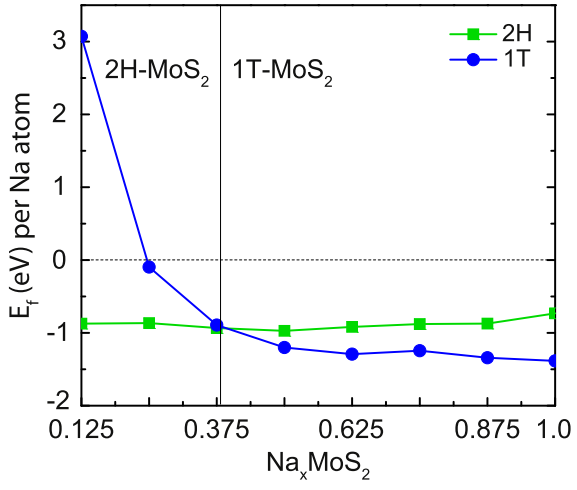

Fig. 5. Formation energy per Na atom for 2H- and 1T-Na_xMoS_2 as a function of Na concentration.

3.4. Charge transfer and electronic structure of Na_xMoS_2

Next we analyze the nature of chemical bonding between Na and host MoS_2 and the electronic structure of the intercalation compounds. Fig. S4 in the SD shows a typical distribution of the charge density difference in Na intercalated layered MoS_2. From the charge density distribution, the net charge on Na was obtained using Bader charge population analysis. Table 1 shows the net charge on Na for low-energy configurations of 2H- and 1T-Na_xMoS_2. In each case, it is evident that Na donates a large fraction of its valence electron indicating a strong ionic character of the bond between Na and the host MoS_2. Next, we calculated the total density of states to analyze the changes in electronic structure of MoS_2 upon Na intercalation as a result of the charge transfer. Fig. 6 shows the concentration-dependent density of states for 2H- and 1T-Na_xMoS_2. It is clear that the electronic structure of 2H-Na_xMoS_2 switches from semiconducting to metallic upon initial Na intercalation, and thereafter remains metallic upon further intercalation. On the other hand, the metallic 1T-MoS_2 is found to remain metallic over a large concentration range. Interestingly, at full concentration ($x = 1$) 1T-MoS_2 demonstrates a band gap in excess of 0.98 eV. This unexpected phenomena can be attributed to the distortion of Mo coordination at very large concentration of available electrons. Similar unexpected changes in electronic structures during intercalation have also been observed in a few electrode materials for LIBs, and can potentially be mitigated by using dopants to increase conductivity of the host material [43–45].

3.5. Electrochemical properties of Na-intercalated MoS_2

In order to examine the suitability of layered MoS_2 as an electrode material for NIBs, we next evaluate its crucial electrochemical characteristics such as voltage profile, specific capacity and Na diffusion barriers. For every concentration x of the Na_xMoS_2 compound, the electrode potential V with respect to Na/Na^+ is calculated as [46,47],

$$V = -\frac{E(x_2) - E(x_1) - (x_2 - x_1)E\left(Na^{bcc}\right)}{e(x_2 - x_1)}$$

where $E(x_2)$ and $E(x_1)$ are the total energies of the Na_xMoS_2 compound at two adjacent low-energy concentrations x_2 and x_1 along the computed convex hull shown in Fig. 3, and $E(Na^{bcc})$ is the energy per atom of Na in the bcc crystal. Fig. 7 shows the concentration-dependent profile of the electrode potential for both 2H and 1T-MoS_2 polytypes. We find that the electrode potential for 2H-Na_xMoS_2 varies in a range of 0–1 V with a decreasing trend with increasing capacity, with an average value of 0.75 V. This observation is qualitatively similar to the measurements of electrode

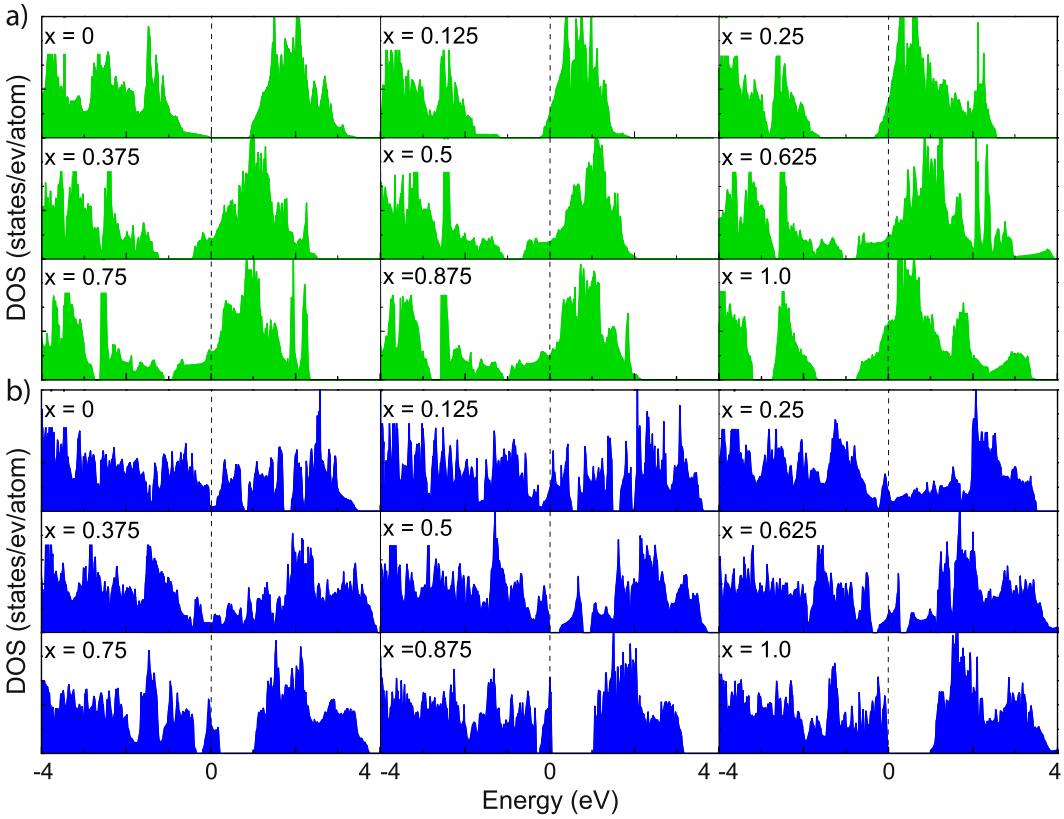

Fig. 6. Total density of states for (a) 2H-Na_xMoS_2 and (b) 1T-Na_xMoS_2. The Fermi level is set to zero eV in each case.

potential upon discharge as reported in the recent work on Na intercalation in MoS_2 [16]. On the other hand, the voltage profile for 1T-Na_xMoS_2 as shown in Fig. 7(b) varies in a broader range. The larger magnitude of the concentration-dependent voltages for 1T-Na_xMoS_2 can be ascribed to the stronger binding of Na with 1T-MoS_2. However, as shown in Fig. 5, 1T-Na_xMoS_2 compounds are unstable for concentrations $x < 0.25$. Therefore, the large magnitudes of the potential of 1T-Na_xMoS_2 for low concentrations are likely to remain inaccessible. Considering stable compositions of 1T-Na_xMoS_2, the average potential is obtained as 1.25 V. Interestingly, the average potential of Na-intercalated MoS_2 is much lower than Li-intercalated MoS_2 (2.0 V) due to the relatively weaker binding of Na compared with Li [15,25]. Since ideally a good anode should have a low electrode potential, our calculated voltage profile in Fig. 7 suggests that layered MoS_2 is suitable as an anode for an NIB. When this Na-intercalated MoS_2 anode is combined with high capacity cathode materials such as $Na_{1.5}VPO_{4.8}F_{0.7}$ and $Na_3MnPO_4CO_3$, the Na-ion battery cell can yield a desirable open circuit voltage in the range of 2.5–3.5 V [48,49].

From our calculations, we also obtained the maximum and the average theoretical specific capacity of Na-intercalated MoS_2 to be 146 mAh g^{-1} and 86 mAh g^{-1}, respectively. Our calculated values on the specific capacities as well as the voltages are comparable to the recent electrochemical measurements, which reported a steady state capacity of 84 mAh g^{-1} in the voltage range of 0.8–1.2 V [16]. This reasonably good agreement between the measured and calculated electrochemical characteristics of layered MoS_2 indicates an ability to achieve an electrochemical performance close to its theoretical maximum. Furthermore, our results on electron charge transfer indicate that Na atoms donate a large fraction of their valence electron to 2H and 1T polytypes (see Table 1). This large electron donation suggests the nature of the bond between of Na atoms and MoS_2 to be of the ionic character. To estimate the ease of this charge transfer during cyclic Na insertion/deinsertion in layered MoS_2, we have used chemical hardness, a metric that evaluates cycling performance efficiency [50]. Consistent with earlier calculations [51], a low value (in the range of 0.04–0.08 eV) for the chemical hardness of the Na intercalation in layered MoS_2, point out to the easiness of charge transfer upon Na intercalation.

One of the crucial characteristics for evaluating suitability of an electrode material for rechargeable batteries is the charge–discharge rate, which depends on the mobility of the intercalating ion. In order to estimate the mobility of Na in MoS_2, we have identified its diffusion path and calculated the associated diffusion barriers using the climbing-image nudged elastic band method [52]. For 2H- and 1T-MoS_2, we considered diffusion of an Na ion in the interlayer van der Waals spaces for concentrations $x = 0.125$ and $x = 0.5$, respectively. Fig. 8c shows the diffusion path between neighboring low-energy octahedral sites and the associated energy profile. In both cases, the path passes through the high energy tetrahedral binding site, with diffusion barrier being 0.68 eV and 0.28 eV for 2H and 1T-MoS_2, respectively. It is evident that an increased Na–Na interaction at higher concentrations leads to a faster Na diffusion in 1T-MoS_2. The Na diffusion barrier in 1T-MoS_2 is smaller than Li diffusion barrier in graphite (0.4 eV) [53] and is comparable to Na diffusion barrier in layered cathode materials such as $NaMPO_4F$ (M = Fe, $Fe_{0.5}Mn_{0.5}$, Mn) and layered $NaCoO_2$ (0.3 eV) [1,54]. Although the Na migration barrier in 2H-MoS_2 is larger, 2H-MoS_2 still offers better mobility in comparison with a number of electrode materials such as post-spinel phases of $CaMn_2O_4$ and $CaTi_2O_4$ with diffusion barriers in excess of 1.0 eV [55]. Since the rates of diffusion in layered MoS_2 is limited by the ability of van der Waals spaces to accommodate Na ions, their mobilities can be further enhanced by using composites of monolayer MoS_2 as suggested by recent experiments [20,21].

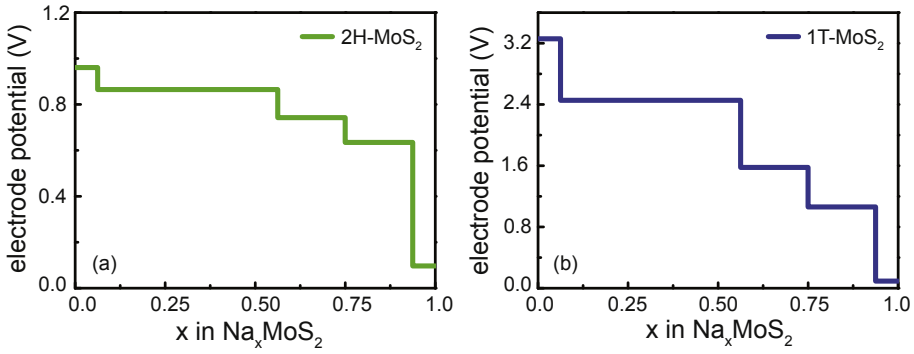

Fig. 7. Electrode potential of Na-intercalated (a) 2H-MoS_2, (b) 1T-MoS_2 against Na/Na^+.

In the preceding section, we have focused on Na intercalation in layered MoS_2 in the concentration range of $0 < x < 1$. Recent studies investigating Li–MoS_2 intercalates have reported that once all interlayer binding sites have been fully occupied with Li, further intercalation at higher concentrations ($x > 1$) leads to the destruction of layered structure of MoS_2 and a loss of cyclic reversibility [33]. This behavior arises due to inversion-type reactions that involve breaking of Mo–S bonds and the formation of lithium sulphides [33,15]. While similar inversion reactions have not yet been reported in case of Na intercalation in MoS_2, it is nevertheless worth analyzing their reaction energetics considering close magnitudes of the electronegativities of Na and Li. We therefore calculated the reaction energies (ΔE_R), defined as the difference between the energy of the products and the reactants, of the following two reactions: $Na + NaMoS_2 \rightarrow 2NaS + Mo$, $\Delta E_R = -12.36$ eV, and $3Na + NaMoS_2 \rightarrow 2Na_2S + Mo$, $\Delta E_R = -15.46$ eV. Large negative energies of these reactions, especially when compared with the formation energies of Na_xMoS_2 intercalation compounds, suggest a likelihood of Na-induced bond breaking in the host MoS_2 at large Na concentrations and the subsequent loss of charge–discharge reversibility. Severe structural distortions at later stages of Na intercalation in MoS_2 as reported in the recent experiments could possibly be attributed to such Na-induced inversion reactions discussed here [16]. In light of the promising electrochemical properties of Na_xMoS_2 as an anode material for Na concentrations in the range of $0 < x < 1$, these irreversible reactions highlight the need for limiting Na concentrations in this range, and motivate the development of inhibitor dopants that can impede the onset of such reactions.

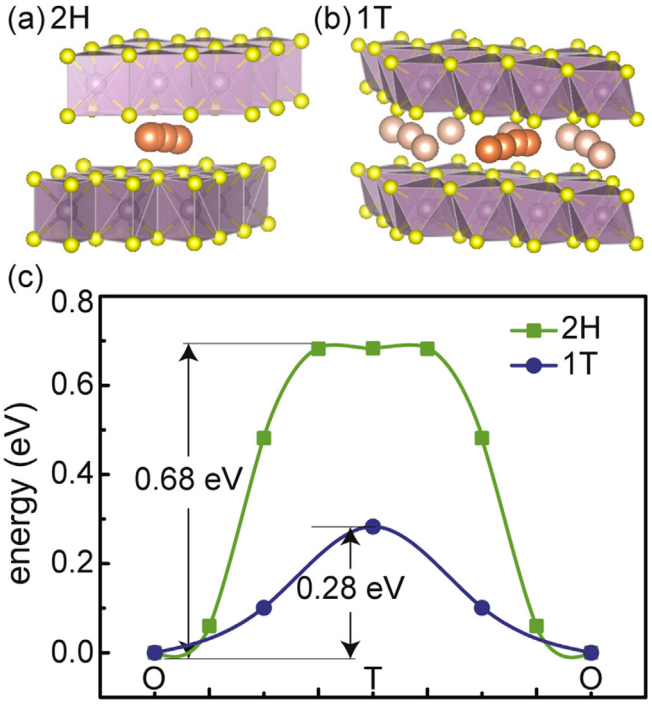

Fig. 8. Schematic illustration of the diffusion path for Na ion in (a) 2H- and (b)1T-MoS_2, from a low-energy octahedral (O) site to its neighboring octahedral site via a tetrahedral (T) site, and (c) associated energy profiles along the path O → T → O.

4. Conclusions

In summary, we have systematically investigated Na intercalation in all structural polytypes of MoS_2. Na ions are generally found to occupy octahedral or distorted octahedral sites within the interlayer van der Waals spaces upon intercalation. The intercalation of Na in MoS_2 causes a phase transformation at $x = 0.39$ from the 2H to 1T phase. However, we find that Na intercalation in MoS_2 is thermodynamically stable across the entire concentration range of $0 < x < 1$ against the phase separation of Na. Furthermore, Na_x-MoS_2 compounds are generally metallic with a low average electrode potential of 0.75–1.25 V and a maximum specific capacity of 146 mAh g^{-1}. Finally, our calculated energy barrier of 0.68 and 0.28 eV for Na diffusion in 2H- and 1T-MoS_2 suggests a moderately fast charge and fast discharge rates, respectively. These results suggest that 1T polytype has better electrochemical performance due to its inherent metallic electronic structure, higher capacity for Na ions and their faster mobilities.

Since the capacity of layered MoS_2 is limited by the ability of van der Waals interlayer space to accommodate Na ions, exfoliating layered structure into individual monolayers can allow for an enhanced adsorption of Na ions on both sides and faster diffusion rates as hinted in some recent experiments [20,21,56]. Similarly using nanorstructures of MoS_2 (such as nanosheets, nanowires and nanoribbons) in combination with composites may also lead to an increase in Na amount adsorbed per MoS_2 formula unit to enhance the specific capacity. Finally, given the close structural and chemical similarities between MoS_2 and other transition metal dichalcogenides such as WS_2, $MoSe_2$ and WSe_2, our study should motivate a thorough investigation of Na intercalation in several transition metal dichalcogenides. Considering that graphite, the widely used layered material as electrodes in rechargeable batteries, is not amenable to Na intercalation, our study suggests the family of transition metal dichalcogenides as promising candidates for anodes of NIBs for stationary energy storage.

Acknowledgment

MM, CW, JD and NM gratefully acknowledge the computational support from the Monash e-Research Centre, iVEC at iVEC@Murdoch and the National Computational Infrastructure. VS gratefully acknowledges support from the National Science Foundation and the U.S. Department of Energy.

Appendix A. Supplementary data

Supplementary data related to this article can be found at http://dx.doi.org/10.1016/j.jpowsour.2014.06.049.

References

[1] S. Ong, V. Chevrier, G. Hautier, A. Jain, C. Moore, S. Kim, X. Ma, G. Ceder, Energy Environ. Sci. 4 (2011) 3680–3688.
[2] S.-W. Kim, D.-H. Seo, X. Ma, G. Ceder, K. Kang, Adv. Energy Mater. 2 (2012) 710–721.
[3] V. Palomares, M. Casas-Cabanas, E. Castillo-Martínez, M.H. Han, T. Rojo, Energy Environ. Sci. 6 (2013) 2312–2337.
[4] T. Yamamoto, T. Nohira, R. Hagiwara, A. Fukunaga, S. Sakai, K. Nitta, S. Inazawa, J. Power Sources 217 (2012) 479–484.
[5] R. Yazami, P. Touzain, J. Power Sources 9 (1983) 365–371.
[6] R. Asher, J. Inorg. Nucl. Chem. 10 (1959) 238–249.
[7] Y. Wang, J.Z. Ou, S. Balendhran, A.F. Chrimes, M. Mortazavi, D.D. Yao, M.R. Field, K. Latham, V. Bansal, J.R. Friend, et al., ACS Nano 7 (2013) 10083–10093.
[8] Q.H. Wang, K. Kalantar-Zadeh, A. Kis, J.N. Coleman, M.S. Strano, Nat. Nanotechnol. 7 (2012) 699–712.
[9] S. Bertolazzi, J. Brivio, A. Kis, ACS Nano 5 (2011) 9703–9709.
[10] J. Li, N.V. Medhekar, V.B. Shenoy, J. Phys. Chem. C. 117 (2013) 15842–15848.
[11] J. Wilson, A. Yoffe, Adv. Phys. 18 (1969) 193–335.
[12] M. Chhowalla, H.S. Shin, G. Eda, L.-J. Li, K.P. Loh, H. Zhang, Nat. Chem. 5 (2013) 263–275.
[13] G. Du, Z. Guo, S. Wang, R. Zeng, Z. Chen, H. Liu, Chem. Commun. 46 (2010) 1106–1108.
[14] T. Stephenson, Z. Li, B. Olsen, D. Mitlin, Energy Environ. Sci. 7 (2014) 209–231.
[15] X. Fang, C. Hua, X. Guo, Y. Hu, Z. Wang, X. Gao, F. Wu, J. Wang, L. Chen, Electrochim. Acta 81 (2012) 155–160.
[16] J. Park, J. Kim, J. Park, T. Nam, K. Kim, J. Ahn, G. Wang, H. Ahn, Electrochim. Acta 92 (2013) 427–432.
[17] Y. Liao, K.-S. Park, P. Xiao, G. Henkelman, W. Li, J.B. Goodenough, Chem. Mater. 25 (2013) 1699–1705.
[18] D. Su, S. Dou, G. Wang, Chem. Commun. 50 (2014) 4192–4195.
[19] H.-S. Ryu, J.-S. Kim, J.-S. Park, J.-W. Park, K.-W. Kim, J.-H. Ahn, T.-H. Nam, G. Wang, H.-J. Ahn, J. Electrochem. Soc. 160 (2013) A338–A343.
[20] L. David, R. Bhandavat, G. Singh, ACS Nano 8 (2014) 1759–1770.
[21] G.S. Bang, K.W. Nam, J.Y. Kim, J. Shin, J.W. Choi, S.-Y. Choi, ACS Appl. Mater. Interfaces 6 (2014) 7084–7089.
[22] F. Wypych, T. Weber, R. Prins, Chem. Mater. 10 (1998) 723–727.
[23] S. El-Mahalawy, B. Evans, Phys. Status Solidi (b) 79 (1977) 713–722.
[24] L. Houben, A. Enyashin, Y. Feldman, R. Rosentsveig, D. Stroppa, M. Bar-Sadan, J. Phys. Chem. C. 116 (2012) 24350–24357.
[25] A. Enyashin, G. Seifert, Comput. Theor. Chem. 999 (2012) 13–20.
[26] G. Kresse, J. Furthmüller, Phys. Rev. B 54 (1996) 11169.
[27] J. Perdew, K. Burke, M. Ernzerhof, Phys. Rev. Lett. 77 (1996) 3865–3868.
[28] P. Blöchl, Phys. Rev. B 50 (1994) 17953.
[29] S. Grimme, J. Comput. Chem. 27 (2006) 1787–1799.
[30] F. Wypych, R. Schöllhorn, J. Chem. Soc. Chem. Commun. (1992) 1386–1388.
[31] L. Mattheiss, Phys. Rev. B 8 (1973) 3719.
[32] P. Raybaud, J. Hafner, G. Kresse, H. Toulhoat, J. Phys. Condens. Matter 9 (1997) 11107.
[33] C. Julien, Mater. Sci. Eng. R. 40 (2003) 47–102.
[34] A. Enyashin, L. Yadgarov, L. Houben, I. Popov, M. Weidenbach, R. Tenne, M. Bar-Sadan, G. Seifert, J. Phys. Chem. C. 115 (2011) 24586–24591.
[35] L. Beaulieu, K. Eberman, R. Turner, L. Krause, J. Dahn, Electrochem. Solid-State Lett. 4 (2001) A137–A140.
[36] M. Mortazavi, J. Deng, V. Shenoy, N. Medhekar, J. Power Sources 225 (2012) 207–214.
[37] L. Beaulieu, T. Hatchard, A. Bonakdarpour, M. Fleischauer, J. Dahn, J. Electrochem. Soc. 150 (2003) A1457–A1464.
[38] J. Wang, X. Liu, S. Mao, J. Huang, Nano Lett. 12 (2012) 5897–5902.
[39] M. Ebner, F. Marone, M. Stampanoni, V. Wood, Science 342 (2013) 716–720.
[40] M. Py, R. Haering, Can. J. Phys. 61 (1983) 76–84.
[41] Y.-C. Lin, D.O. Dumcenco, Y.-S. Huang, K. Suenaga, Nat. Nanotechnol. 9 (2014) 391–396.
[42] W. Zhou, Nat. Nanotechnol. 9 (2014) 333–334.
[43] X. Rocquefelte, F. Boucher, P. Gressier, G. Ouvrard, P. Blaha, K. Schwarz, Phys. Rev. B 62 (2000) 2397.
[44] M. Torabi, S. Sadrnezhaad, J. Power Sources 196 (2011) 399–404.
[45] G. Lu, S. Qiu, J. Liu, X. Wang, C. He, Y.-J. Bai, Electrochim. Acta 117 (2014) 230–238.
[46] M. Aydinol, A. Kohan, G. Ceder, K. Cho, J. Joannopoulos, Phys. Rev. B 56 (1997) 1354.
[47] M. Aydinol, A. Kohan, G. Ceder, J. Power Sources 68 (1997) 664–668.
[48] Y.-U. Park, D.-H. Seo, H.-S. Kwon, B. Kim, J. Kim, H. Kim, I. Kim, H.-I. Yoo, K. Kang, J. Am. Chem. Soc. 135 (2013) 13870–13878.
[49] H. Chen, Q. Hao, O. Zivkovic, G. Hautier, L.-S. Du, Y. Tang, Y.-Y. Hu, X. Ma, C.P. Grey, G. Ceder, Chem. Mater. 25 (2013) 2777–2786.
[50] R. Parr, P. Chattaraj, J. Am. Chem. Soc. 113 (1991) 1854–1855.
[51] X. Chen, J. He, D. Srivastava, J. Li, Appl. Phys. Lett. 100 (2012) 263901–263904.
[52] G. Henkelman, B.P. Uberuaga, H. Jónsson, J. Chem. Phys. 113 (2000) 9901.
[53] K. Persson, Y. Hinuma, Y.S. Meng, A. Van der Ven, G. Ceder, Phys. Rev. B 82 (2010) 125416.
[54] R. Tripathi, S.M. Wood, M.S. Islam, L.F. Nazar, Energy Environ. Sci. 6 (2013) 2257–2264.
[55] C. Ling, F. Mizuno, Chem. Mater. 25 (2013) 3062–3071.
[56] J. Xiao, D. Choi, L. Cosimbescu, P. Koech, J. Liu, J.P. Lemmon, Chem. Mater. 22 (2010) 4522–4524.